RSC Advances

ROYAL SOCIETY OF CHEMISTRY

www.rsc.org/advances

Preparation of lepidocrocites with different degrees of crystallization and their photocatalytic properties

Rufen Chen*[a], Shuangfei Zhao[a], Xiangmin Meng[b], Hui Liu[a], Yu Wei*[,a]

(a.College of Chemistry and Material Science, Hebei Normal University, Shijiazhuang, 050024, P.R.China)

(b.Key Laboratory of Photochemical Conversion and Optoelectronic Materials, TIPC, Chinese Academy of Sciences, Bejing, 100190, P.R. China)

Abstract: This paper describes the preparation of lepidocrocites (γ-FeOOH) via the air oxidation of $Fe(OH)_2$ under visible light irradiation in the presence of oxalic acid. Experimental results show that lepidocrocites with different degrees of crystallization can be obtained by controlling the concentration of oxalic acid under visible light irradiation. The crystallization of γ-FeOOH is found to gradually decrease with increase in the concentration of oxalic acid. This provides an alternative approach for the synthesis of low-crystalline γ-FeOOH. Based on the results, a possible oxidation mechanism of Fe(II) has been proposed, which involves the formation of an Fe(II)-oxalate complex under light irradiation to produce oxidizing species, leading to an increase of the oxidation rate. The higher oxidation rate favors the formation of low-crystalline γ-FeOOH. In contrast to the high-crystalline γ-FeOOH, the low-crystalline γ-FeOOH with high specific surface shows higher adsorption and photocatalytic activity toward the photodegradation of orange II.

Keywords: Different crystallized γ-FeOOH; Visible light; Oxalic acid; Photocatalytic activity

---

* Corresponding author. Tel.: 86031170787400, fax: 86031170787400.

E-mail: rufenchen7@gmail.com(R. Chen), weiyu@mail.hebtu.edu.cn(Y. Wei).

1. Introduction

Iron oxides, specifically hydroxides and oxyhydroxides, find applications in pigments, anticorrosion paints, and catalysts, among others. Most iron oxides are semiconductors, capable of exhibiting photocatalytic activity under solar irradiation.[1-2] Iron oxides and polycarboxylic acids can form a photochemical system to realize Fenton-like photodegradation of organic pollutants in aqueous solutions.[3-7] Among the family of polycarboxylic acids, oxalic acid is one of the most active members, with the iron oxide–oxalate complex exhibiting a strong ligand-to-metal charge transformation ability. However, to the best of our knowledge, not many studies have investigated the influence of oxalic acid on the formation of iron oxides.

Among the different iron oxides, lepidocrocite (γ-FeOOH) has been widely used as a functional material in Fenton-like reactions and photocatalytic processes for environmental remediation applications, including the photodegradation of organic dyes, as well as the photolysis of heavy metal salts.[8-10] Given these advantages, the preparation of highly active γ-FeOOH is important in the field of modern materials chemistry. According to our previous studies, both visible light and the presence of trace amounts of ethylenediaminetetracetic acid (EDTA) could increase the reaction rate of γ-FeOOH. The relatively high oxidation rate favors the formation of highly active, low-crystalline γ-FeOOH phase, which readily transforms to α-Fe_2O_3.[11-12] However, the influence of oxalic acid on the formation of γ-FeOOH and the photocatalytic properties of γ-FeOOH under visible light irradiation needs further discussion.

In this study, we demonstrate the preparation of γ-FeOOH by air oxidation of the $Fe(OH)_2$ under visible light irradiation in the presence of trace amounts of oxalic acid at room temperature. In addition, we discuss the mechanism underlying the oxidation of Fe(II) and the photocatalytic activity of γ-FeOOH.

2. Experimental Section

2.1. Materials

Sodium hydroxide (NaOH), oxalic acid, sulfuric acid (H_2SO_4), 30 wt% hydrogen peroxide (H_2O_2), p-benzoquinone (BZQ), disodium ethylenediaminetetraacetate (Na_2-EDTA), tert-butanol and orange II were purchased from Tianjin Chemical Reagents Company (the purities are 99%), and were used as received without further purification. Aqueous ferrous sulfate ($FeSO_4$) solution was prepared by dissolving iron granule in 20% H_2SO_4. Distilled water was used as solvent for the reactions.

2.2. Preparation of γ-FeOOH samples

The standard procedure was as follows. Different volumes (0, 6, 10, and 16 mL, respectively) of a 0.05 M oxalic acid solution were added to well-stirred aliquots (10.0 mL) of a 1 M aqueous solution of $FeSO_4$ in a 250 mL beaker. The mixtures were adjusted to pH 8.7 by adding 6.0 M NaOH. The volume of each solution was adjusted to 100 mL with distilled water. The concentrations of oxalic acid in the mixtures were 0.0, 3.0, 5.0, and 8.0 mM, respectively. Each beaker was in turn placed in a double-walled quartz cooling water jacket, by which the temperature of each reaction mixture was maintained at 20±1 ºC. The reactor was placed at a fixed distance of 10 cm from the lamp. Incandescent lamps were used as light sources. The wavelengths of the lamps were about 400–750 nm. The light intensity (E) was detected by means of a light meter (TES-1336A). Air at flow rate (0.272 $m^3 \cdot h^{-1}$) was then pumped into the suspensions under visible light irradiation. The mixtures were stirred during the reaction process. The suspension was changed to dark green in color (green rust Ⅱ) from an initial white color ($Fe(OH)_2$) and changed to a brown color as the reaction continued. The concentration of Fe (Ⅱ) (solid and liquid) was monitored during the oxidation (15 mL of the suspension was taken out at different time and dissolved in 20% H_2SO_4, determined by the 1,10-phenanthroline method [13-15]). The H_2O_2 concentration in the solution was determined using a H_2O_2 - photometer (Lovibond ET-8600 Germany) at LED 528 nm. The precipitate was collected by

filtration and washed with distilled water and $NH_3 \cdot H_2O$ (1M) and then dried in an oven (40～50 ºC) for 24 h.

2.3 Adsorption experiments

The adsorption experiments of orange II on the γ-FeOOH surface were conducted at 20 °C in the dark at pH 4. A fixed amount of γ-FeOOH (0.2 g) was added to 100 mL of an aqueous orange II solution with various concentrations, which remained for 6 h in a vibrator unit in the dark under N_2 at 20 °C. Orange II concentrations were measured after equilibrium by a spectrophotometer (SP-752, Shanghai) at a wavelength of 580 nm, using a 1 cm quartz cell, and the amount of orange II adsorbed on the γ-FeOOH was calculated based on the mass balance according to Eq. (6).[16]

2.4 Measurement of photocatalytic activity

The photocatalytic degradation of orange II using different crystallized γ-FeOOH was carried out at pH 4 as follows. A fixed amount of γ-FeOOH (0.2 g) was added to 100 mL of orange II solution (20 u M). The dye and γ-FeOOH were stirred for 30 min in the dark to ensure adsorption equilibrium. H_2O_2 was added to the reaction vessel at the beginning of the irradiation by a 100 W incandescent lamp. At selected time intervals, 5 mL aliquots were collected, filtered. All experimental runs were performed at 20 ◦C under continuous stirring in the presence of visible light and air. The concentrations of orange II in the filtrates were measured by a UV-Visible spectrophotometer at 486nm. And the H_2O_2 concentrations in the filtrates were determined using a H_2O_2 – photometer at LED 528 nm. The degradation efficiency of orange II and the decomposition efficiency of H_2O_2 could be calculated from the following equation:

$$\text{Degradation efficiency of orange II (Decomposition efficiency of } H_2O_2\text{) (\%)} = \frac{C_0 - C}{C_0} \times 100;$$

where C_0 and C represent the concentrations of the orange II (H_2O_2) at the start of reaction and after reaction, respectively. The concentration of Fe(III) and Fe(II) in solution were determined by the 1,10-phenanthroline method.[15]

2.5 Sample characterizations

X－ray diffraction (XRD) patterns were obtained on a Bruker diffractometer D8 ADVANCE using a Cu Kα radiation. The images of samples were obtained by low- resolution Transmission electron microscopy (TEM, Hitachi H-7500) and high resolution transmission electron microscopy (HRTEM, JMS 2011) with an accelerating voltage of 200kV. IR spectra were recorded on a FTIR-8900 Fourier transform infrared spectroscope in KBr pellets. UV–vis diffuse reflectance spectra (UVDRS) were obtained using a UV–vis spectrometer (U-3010, Hitachi) equipped with an integrating sphere assembly. The specific surface area of the iron oxides was determined by multipoint N_2-BET analysis using a Quantachrome (NOVAe) surface area analyzer.

3. Results and Discussion

3.1 Effects of oxalic acid and visible light on the products

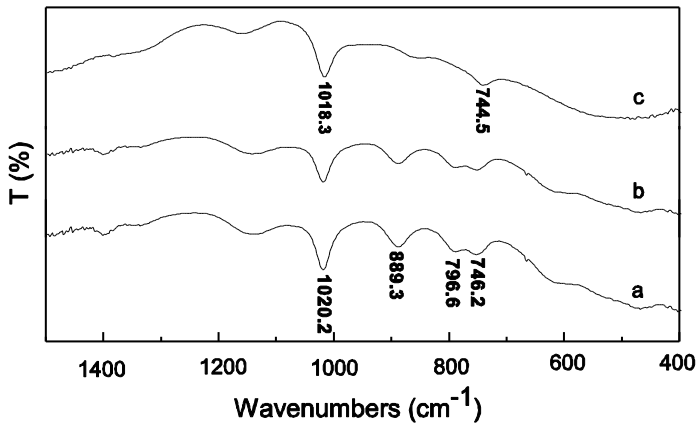

Fig.1 IR spectra of the products at different light intensities with and without oxalic acid

(a: E= 1000lux, C=0 mM; b: E=0 lux, C= 3 mM; c:E=1000 lux, C= 3 mM)

The influence of oxalic acid and visible light on the formation of the products was investigated. We simulated a dark reaction to understand the kinetics of the oxidation process. Fig. 1 shows the IR

spectra of the three reaction products obtained by irradiation under different intensities of light (E), with and without oxalic acid (oxalic acid concentration is denoted as C). For α-FeOOH, the IR bands at 889.3 and 796.6 cm^{-1} correspond to the in-plane and out-of-plane Fe–O–H bending vibrations, respectively. On the other hand, for γ-FeOOH, the IR bands at 1018.3 (1020.2) and 744.5 (746.2) cm^{-1} are assigned to the in-plane and out-of-plane Fe–O–H bending vibrations, respectively.[11,17] The results obtained in this study indicate the formation of phase-pure γ-FeOOH under visible light irradiation in the presence of oxalic acid (Fig. 1c). A mixture of γ-FeOOH and α-FeOOH is formed when the reaction system is short of either oxalic acid or light irradiation.

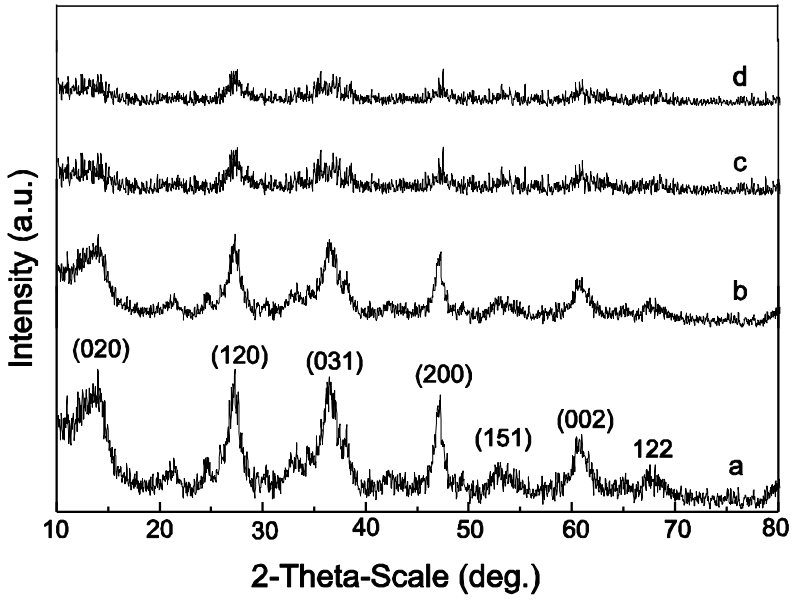

Fig. 2 XRD patterns of samples at different concentrations of oxalic acid under visible light irradiation (a: 3mM; b: 5mM; c: 7mM, d: 9mM)

Furthermore, we investigated the influence of the concentration of oxalic acid on the formation of the oxide phase, under a fixed light irradiation intensity of 1000 lux. Fig. 2 shows the XRD patterns of the as-prepared samples. All diffraction peaks could be unambiguously assigned to the γ-FeOOH phase (JCPDS: 44-1415), indicating that the samples are phase-pure γ-FeOOH with a

layered structure. Meanwhile, the TEM and HRTEM images of the three different lepidocrocites are shown in Fig. 3. HRTEM observation shows that three samples have a certain crystalline. Correlating the results shown in Figs. 2 and 3, it can be realized that the crystallization of γ-FeOOH gradually decreases with increase in the concentration of oxalic acid. In particular, the crystallization of γ-FeOOH is poor for the concentration of oxalic acid greater than or equal to 7 mM.

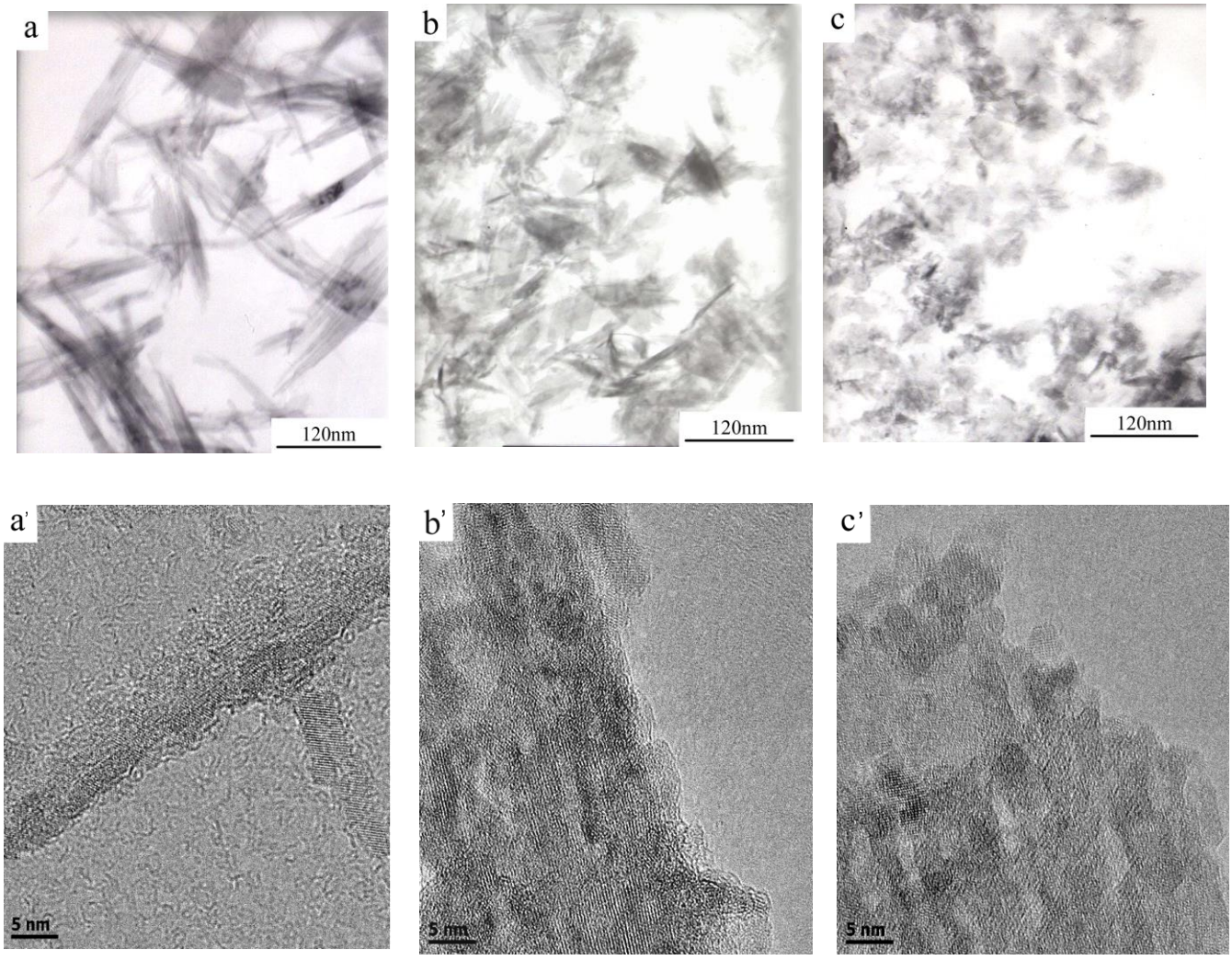

Fig.3 TEM images (a: 3mM; b: 5mM; c: 7mM) and HRTEM images (a': 3mM; b': 5mM; c': 7mM) of samples at different concentrations of oxalic acid under visible light irradiation

The observed variations could be ascribed to the difference in the reaction rates. The concentrations of Fe(II) (solid and liquid) and H_2O_2 in the suspension were determined as a function

of reaction time during oxidation at different light intensities and oxalic acid concentrations (Figs.4 and 5). As shown in Fig. 4(A), the concentration of Fe (Ⅱ) decreases faster for the reaction in the presence of oxalic acid under the light irradiation (Fig. 4(A) c) than short of either oxalic acid or light irradiation (Fig. 4(A) a and b). And the concentration of Fe(II) decreases rapidly in the reaction with increase in the concentration of oxalic acid under the light irradiation (Fig.4(B)).

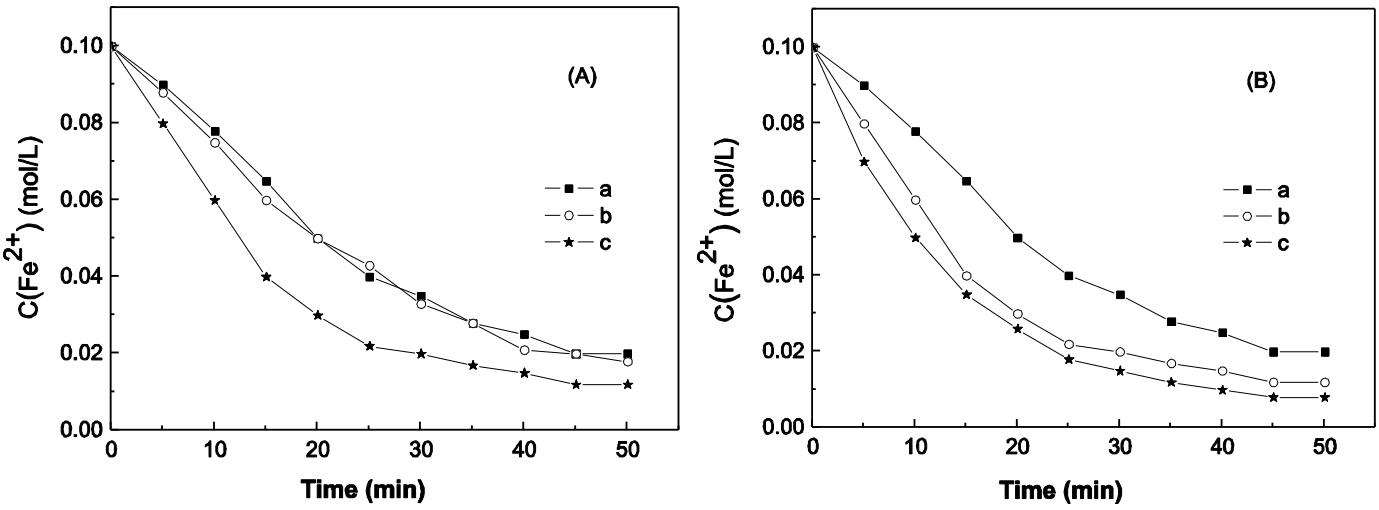

Fig.4 Changes of the Fe (Ⅱ) concentration with reaction time: (A): different light intensities with and without oxalic acid (a: E= 1000lux, 0 mM oxalic acid; b: E=0 lux, 3 mM oxalic acid; c:E=1000 lux, 3 mM oxalic acid); (B): different concentrations of oxalic acid under visible light irradiation （1000 lux）(a: 0 mM oxalic acid; b: 3 mM oxalic acid; c: 7 mM oxalic acid)

Fig. 5(A) and (B) show that the concentrations of H_2O_2 increase with the reaction time, particularly in the earlier stages of the reaction (0–15 min). As the reaction progresses, the concentration of H_2O_2 tends to decrease gradually. This can be explained based on the fact that the H_2O_2 in the system reacts with Fe^{2+} to form iron oxides, thereby leading to the observed decrease in the concentration of H_2O_2 in the later stages of the reaction.[10,18-19] Meanwhile, Fig. 5(A) shows that

the concentration of H_2O_2 increases faster for the reaction in the presence of oxalic acid under the light irradiation (Fig. 5(A) c) than short of either oxalic acid or light irradiation (Fig. 5(A) a and b). And Fig. 5(B) suggests that the addition of oxalic acid under the light irradiation favors the generation of H_2O_2, leading to the increase of H_2O_2 concentration with increase in the concentration of oxalic acid.

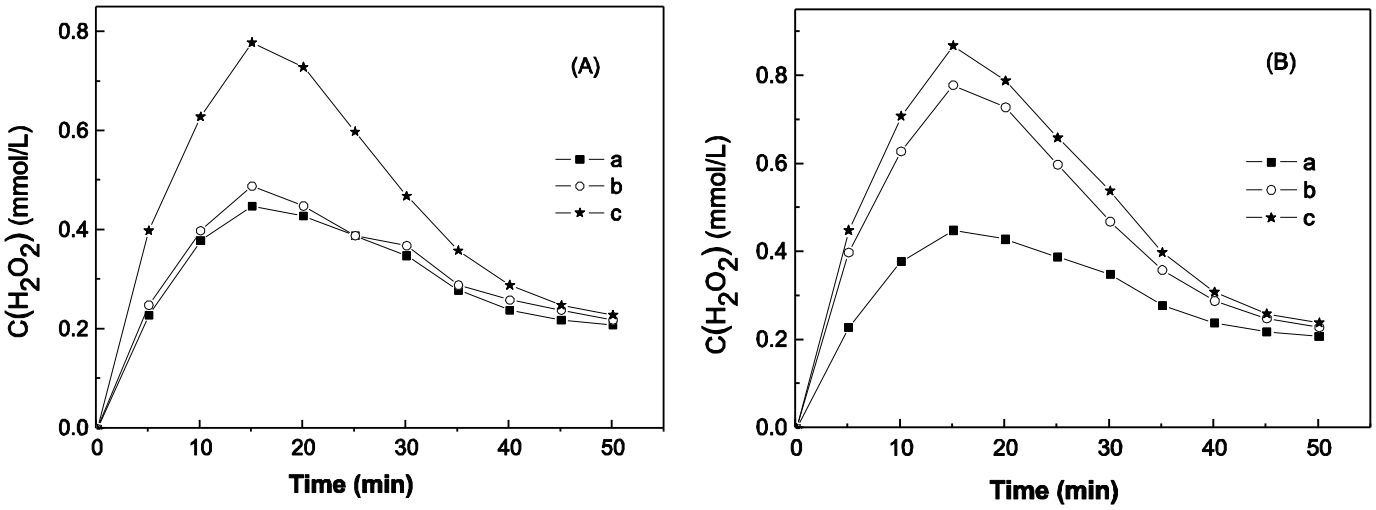

Fig.5 Changes of the H_2O_2 concentration with reaction time: (A): different light intensities with and without oxalic acid (a: E= 1000lux, 0 mM oxalic acid; b: E=0 lux, 3 mM oxalic acid; c:E=1000 lux, 3 mM oxalic acid); (B): different concentrations of oxalic acid under visible light irradiation（1000 lux）(a: 0 mM oxalic acid; b: 3 mM oxalic acid; c: 7 mM oxalic acid)

From Fig. 4 and Fig. 5 we can see that both visible light irradiation and the presence of oxalic acid can accelerate the oxidation of Fe (Ⅱ). And the rate of the oxidation is decreased when the reaction system is short of either oxalic acid or light irradiation. Meanwhile, with increase in the concentration of oxalic acid, the rate of the oxidation is further accelerated under the light irradiation.

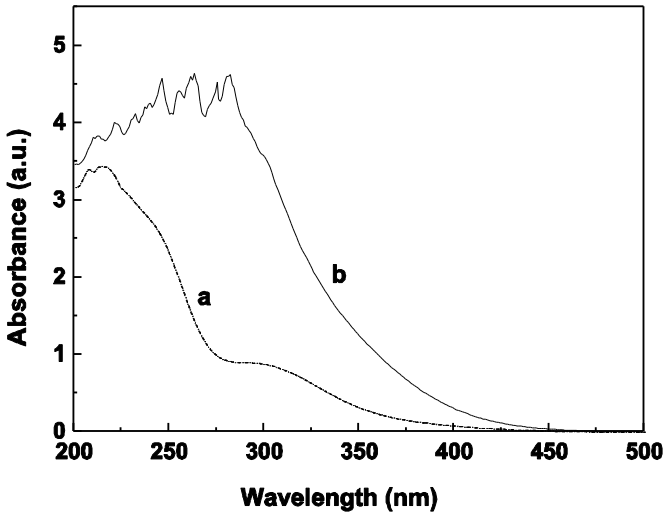

Fig.6 UV-vis absorption spectra of Fe (Ⅱ) and Fe (Ⅱ)-oxalate solution (a: Fe (Ⅱ); b: Fe (Ⅱ)-oxalate)

During the oxidation of Fe(II), oxalic acid chelates Fe(II) to form Fe(II)-oxalate complex, which shows strong absorption bands in the near-UV and visible regions.[20-22] Fig. 6 shows the UV–Vis absorption spectra of Fe(II) and Fe(II)-oxalate solutions. As is seen, the onset of the band-gap transition of Fe(II)-oxalate is indicated by a red shift (Fig. 6b) compared with that of the Fe(II) solution (Fig. 6a). In the reaction system, the Fe(II)-oxalate complex absorbs light in the near-UV and visible regions, during which there is a charge transfer from the ferrous ion to a surrounding solvent molecule, leading to the formation of Fe(III)-oxalate complex and a solvated electron [$e^-_{(aq)}$]. Subsequently, the O_2 molecules in the solution combine with the solvated electron and H^+ to form $O_2^{-\bullet}$ and H_2O_2,[16] which further oxidizes Fe(II) to Fe(III). In addition, hydroxyl radicals (OH•) are formed during the reaction between H_2O_2 and Fe(II), which act as another source of oxidant.[23-24] Thus, the oxidation of Fe(II) to Fe(III) is overall accelerated with increase in the concentration of oxalic acid under visible light irradiation, as shown in Eqs. (1–5)

$$\text{Fe(Ⅱ)-oxalate} \xrightarrow[O_2]{h\nu} \text{Fe (Ⅲ)- oxalate} + e^-_{(aq)} \quad (1)$$

$$O_2 + e^-_{(aq)} \longrightarrow O_2^{-\bullet} \quad (2)$$

$$O_2^{-\bullet} + e^-_{(aq)} + 2H^+ \longrightarrow H_2O_2 \quad (3)$$

$$H_2O_2 + Fe(II) \longrightarrow Fe(III) + OH^- + OH\bullet \quad (4)$$

$$OH\bullet + Fe(II) \longrightarrow Fe(III) + OH^- \quad (5)$$

The oxidation reaction is certainly accelerated due to the action of visible light in the presence of trace amounts of oxalic acid. The formation of γ-FeOOH is favored under such high oxidation conditions.[11,25] In addition, an increase in the concentration of oxalic acid further increases the reaction rate. Consequently, the seed crystals of γ-FeOOH are formed too rapidly. It creates a situation wherein too many seed crystals of γ-FeOOH grow in a short time span. Thus, a rapid reaction rate is favorable for the formation of low-crystalline γ-FeOOH. With further increase in the concentration of oxalic acid, the oxidation is accelerated even further, leading to degradation in the crystallization of γ-FeOOH.

3.2 Adsorption of orange II by lepidocrocites

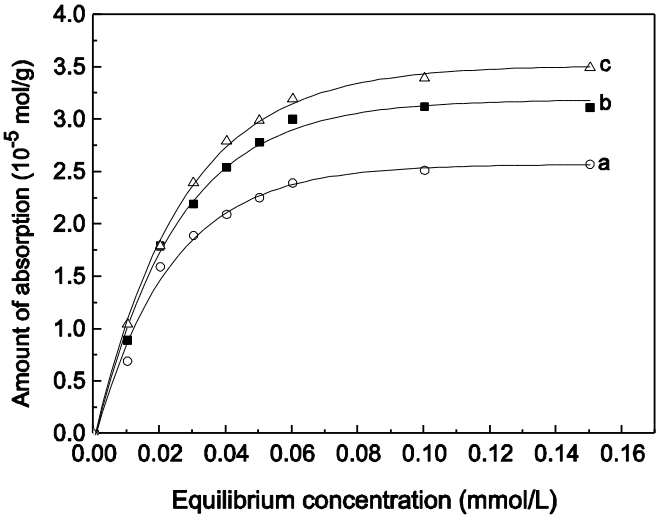

Fig.7 Adsorption isotherms of orange II on the L-3 (a), L-5 (b) and L-7 (c)

As mentioned earlier, three lepidocrocites with different degrees of crystallization were obtained under visible light irradiation by varying the concentration of oxalic acid (3, 5, and 7 mM oxalic acid); the respective samples are denoted as L-3, L-5, and L-7. The adsorption isotherms of orange II on the prepared lepidocrocite samples L-3, L-5, and L-7 are shown in Fig. 7. These isotherms exhibited best fit with the Langmuir adsorption model, as shown in Eq. (6).[10,16]

$$\frac{C_e}{\Gamma} = \frac{1}{\Gamma_{max}} \mathbf{C_e} + \frac{1}{K_\alpha \Gamma_{max}} \quad (6)$$

C_e and Γ_{max} (mol/g) are the adsorbed concentration and saturated adsorption capacity, respectively, and K_a (L/mol) is the adsorption equilibrium constant. The Γ_{max} and K_a values of orange II on the prepared lepidocrocite samples L-3, L-5, and L-7 are listed in Table 1. The Γ_{max} values can be ranked in the order of L-7 > L-5 > L-3, whereas the order of K_a can be ranked as L-7 > L-5 > L-3. In principle, a higher value of physical adsorption corresponds to a larger specific surface area (SSA) and lower crystallization. Similarly, a larger K_a value denotes stronger chemical adsorption.[1,26] Given these considerations, the results obtained in this study imply that the lepidocrocites show higher physical and chemical adsorption with decrease in the degree of crystallization.

Table1 Adsorption parameters of orange II by using the L-3, L-5 and L-7

Samples	SSA (m^2/g)	$\Gamma_{max} \times 10^{-5}$ (mol/g)	$K_a \times 10^4$ (L/mol)	R^2
L-3	139.9	2.502	2.42	0.996
L-5	186.7	3.190	2.80	0.997
L-7	211.6	3.506	2. 86	0.998

3.3 Photocatalytic oxidation of orange II

It is considered that the initial concentration of H_2O_2 is a key factor affecting the photodegradation of orange II in the γ-FeOOH system.[27] Therefore, to gain deeper insights on this

behavior, we performed a set of experiments using orange II and L-7 under visible light irradiation at pH 4, by varying the initial concentration of H_2O_2 from 0 to 5 mM. The corresponding results are shown in Fig. 8. It is quite obvious that the degradation efficiency of orange II increases significantly with the initial concentration of H_2O_2. More quantitatively, almost 85% of orange II is degraded within 5 h of reaction in the presence of 3 mM of H_2O_2. With increase in the concentration of H_2O_2 to greater than 3 mM, there is no significant increase in the degradation efficiency of orange II. It has been reported that the utilization of H_2O_2 decreases with increase in its concentration during the Fenton reaction. In this system, H_2O_2 acts as an effective reagent capturing the photogenerated electron and leading to the formation of OH• as well as a scavenger.[22,26] Considering the trade-off between these two activities, the optimum concentration of H_2O_2 is taken as 3 mM.

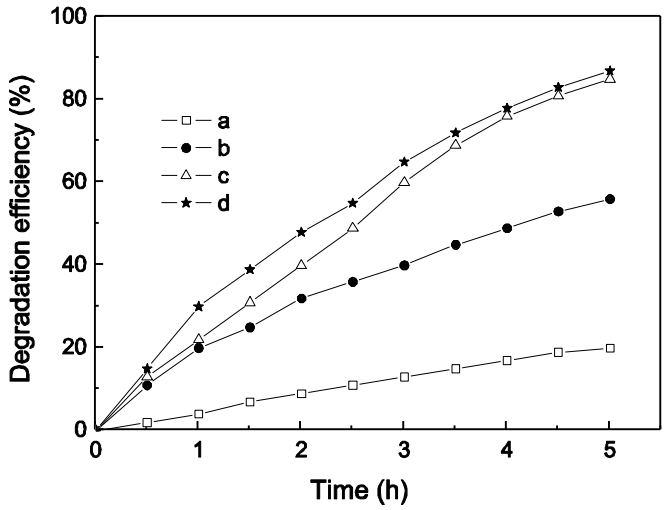

Fig.8 Concentration effects of H_2O_2 on the photodegradation of orange II in the aerated suspension of L-7: (a) 0 mM; (b) 1mM; (c) 3 mM; (d) 5 mM

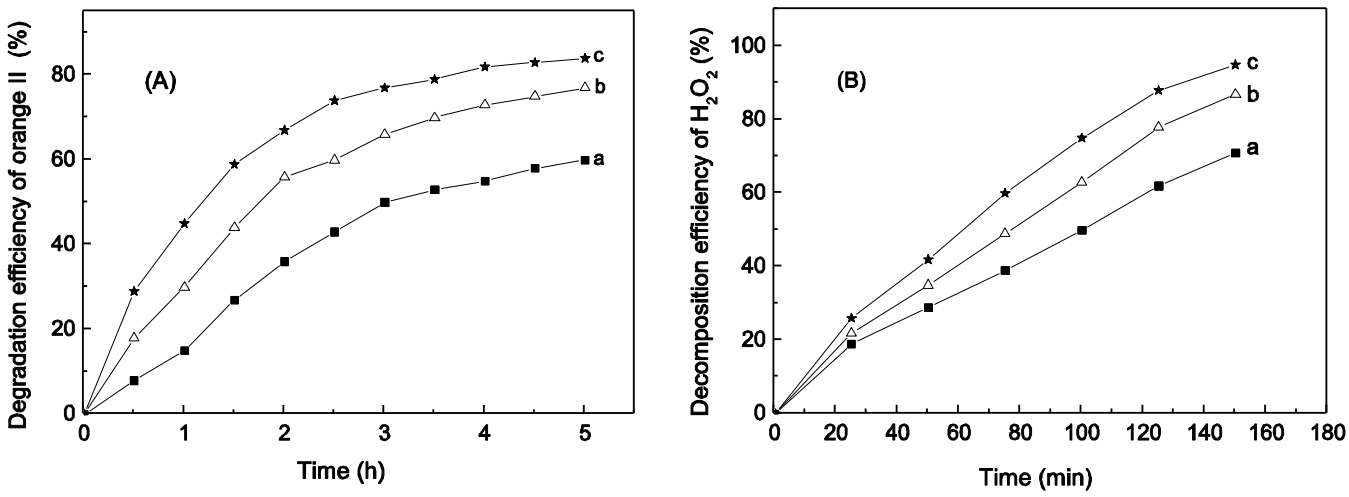

Fig.9 Degradation efficiency of orange II (A) and decomposition efficiency of H_2O_2 (B) with reaction time in the presence of different crystallized lepidocrocites: (a) L-3; (b) L-5; (c) L-7

Fig. 9 (A) shows the degradation of orange II on the different lepidocrocite samples with 3.0 mM of H_2O_2 under visible light irradiation at pH 4. Among these samples, L-7 exhibits the highest degradation efficiency (Fig. 9(A) c) while L-3 exhibits the lowest degradation efficiency (Fig. 9(A) a). It has been confirmed that iron (hydr) oxides can catalyze the decomposition of H_2O_2 and form OH• radicals.[28-29] In our case, H_2O_2 concentrations were determined with reaction time using different crystallized lepidocrocites as the photocatalysts. In Fig.9 (B), the decomposition efficiency of H_2O_2 gradually increases as a function of the reaction time. And the decomposition efficiency of H_2O_2 gradually increases with decrease in the degree of crystallization. The low-crystalline γ-FeOOH shows higher catalytic activity toward the decomposition of H_2O_2. The OH• radicals can be formed with the decomposition of H_2O_2.

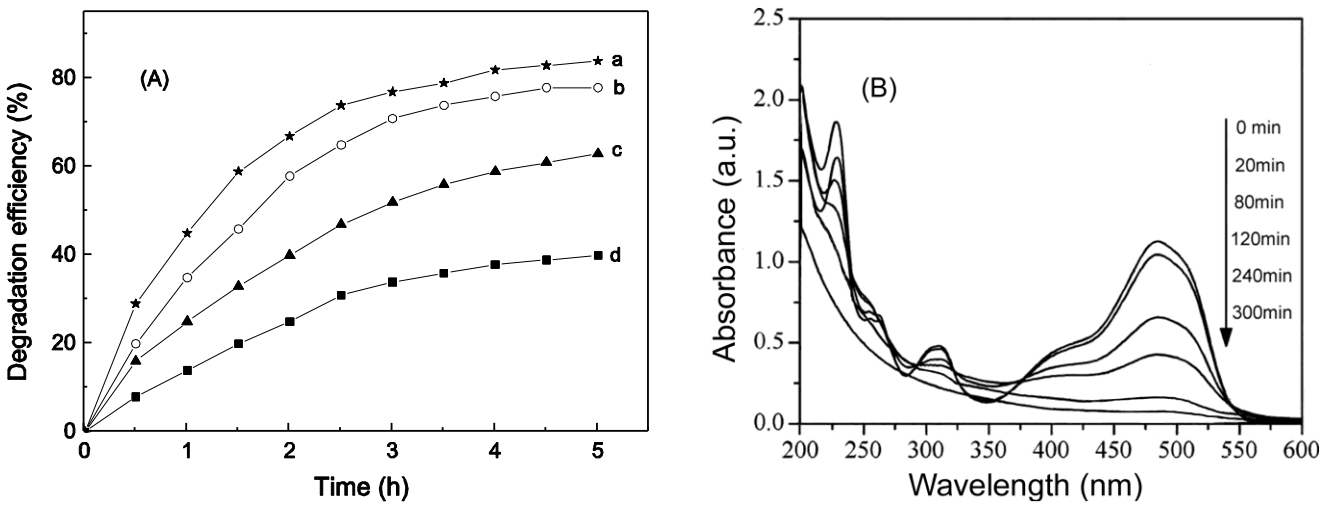

Fig.10 Reactive species trapping experiments in the L-7/H_2O_2 system (A) (a: L-7/H_2O_2; b: L-7/H_2O_2 + 5mM BZQ; c: L-7/H_2O_2 + 5mM Na_2-EDTA; d: L-7/H_2O_2 + tert-butanol); UV-vis spectral changes of Orange II in the L-7/H_2O_2 system (B)

Furthermore, reactive species trapping experiements were performed to investigate active oxidizing species in the L-7 with 3.0 mM of H_2O_2 system under visible light irradiation where three different chemicals, p-benzoquinone (BZQ, a $O_2^{-\bullet}$ radical scavenger), disodium ethylenediaminetetraacetate (Na_2-EDTA, a hole scavenger) and tert-butanol (a OH• radical scavenger), were employed.[30-32] Fig. 10(A) shows that the addition of Na_2-EDTA results in the decrease of photocatalytic activity of the L-7/H_2O_2 system (Fig.10(A)c), the introduction of tert-butanol into the same system causes fast deactivation of photocatalyst (Fig.10(A)d), whereas the presence of BZQ has a small effect on the inactivation of photocatalyst (Fig.10(A)b). Experimental results indicate that active $O_2^{-\bullet}$ radicals, OH• radicals and holes can be produced, and degrade orange II dye in the L-7/H_2O_2 system under visible light irradiation. And the OH• radicals contribute most to the photocatalytic system.

The UV–visible spectral changes observed during the degradation of orange II in the presence of L-7/H_2O_2 system under visible light irradiation, are shown in Fig. 10(B). There are three characteristic absorbance peaks at 228, 310 and 484 nm. The former two peaks derive from aromatic rings, and the latter peak from conjugated structure form by azo bond.[33] The results show that the intensities of the 484 nm absorption peaks decrease rapidly with the reaction proceeding, indicating that the N=N bond of orange II is gradually destructed.[33] As the reaction proceeds, the 228 nm and 310nm absorption peaks, gradually decrease and nearly disappear, showing that aromatic rings are gradually broken.[34]

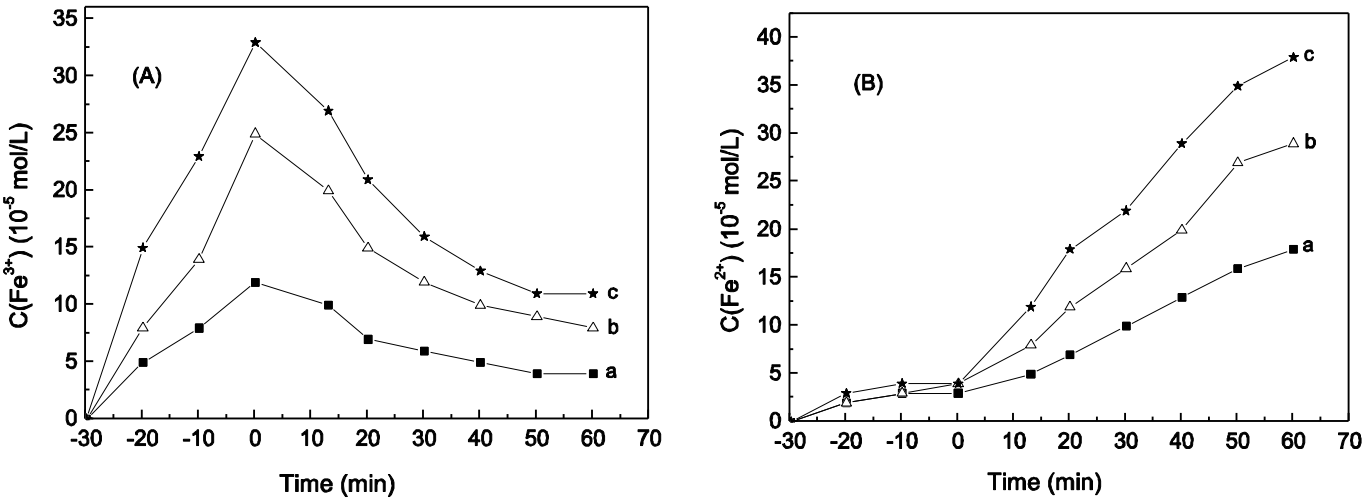

Fig.11 The concentration of the dissolved Fe(III) (A) and Fe(II) (B) vs. reaction time by using different crystallized lepidocrocites :(a) L-3; (b) L-5; (c) L-7

During the photoreaction, iron oxides could be photodissolved. The dissolved Fe(III) species could be photoreduced to generate Fe(II) species.[11] Fig. 11 shows that the concentration of Fe(III) and Fe(II) species in the system of different lepidocrocite samples with 3.0 mM of H_2O_2. As can be seen from Fig. 11(A), the concentration of Fe(III) increases and reaches the maximum after 30 min of dark adsorption in the solution, while the corresponding concentration of Fe(II) is negligible (Fig.

11(B)). This result suggests that the dissolution of γ-FeOOH and subsequent reduction of Fe(III) would have occurred partly in the dark. During the entire photoreaction process, the concentration of Fe(III) decreases constantly, with corresponding increases in the concentration of Fe(II). The observed decrease in the concentration of Fe(III) might be attributed to the photoreduction process. During the reaction under visible light irradiation, the Fe(III) species are readily reduced to form Fe(II). Meanwhile, Fig. 11 also indicates that the concentrations of Fe(III) and Fe(II) species in the system vary as a function of the degree of crystallization of the lepidocrocite sample. It can be observed that the concentrations of Fe(III) and Fe(II) species increase with decrease in the degree of crystallization. This trend is consistent with the order of SSA and saturated adsorption capacity presented in Table 1. The formation of Fe(III) and Fe(II) species during the reaction plays a critical role in the degradation of orange II. In the system, if more Fe(III) species are dissolved during the initial conditions and subsequently photoreduced during the reaction, the system would contain higher concentration of Fe(II). Consequently, the system would exhibit higher efficiency for the degradation of orange II, [35] based on a homogeneous Fenton reaction (Eq. 4).

In addition, the increased adsorption of orange II on the low-crystalline γ-FeOOH is expected to enhance the photodegradation of orange II in the γ-FeOOH/H_2O_2 system.[27] Upon visible light irradiation, electron–hole pairs are photogenerated on the surface of the γ-FeOOH catalyst. The Fe(III)–OH in the system can combine with H_2O_2 to form OH• by heterogeneous Fenton reaction, as shown in Eqs. (7–9).[10, 36]

$$\text{Fe(III)–OH} + h\nu \longrightarrow e_{cb}^{-} + h_{vb}^{+} \quad (7)$$

$$\text{Fe(III)–OH} + H_2O_2 \longrightarrow \text{Fe(II)–OH} + HO_2\bullet \quad (8)$$

$$\text{Fe(II)–OH} + H_2O_2 \longrightarrow \text{Fe(III)–OH} + OH\bullet + HO^{-} \quad (9)$$

Subsequently, the OH• and h_{vb}^{+} formed in the system react with the dye molecules to form other species, and thus are responsible for the dye degradation. The surface-adsorbed organic compounds are readily oxidized by the OH• radicals. Consequently, the low-crystalline γ-FeOOH not only shows

higher adsorption for orange II but also exhibits higher photocatalytic degradation activity. The possible pathway for the photocatalytic degradation of orange II by the γ-FeOOH photocatalyst is shown in Fig. 12.

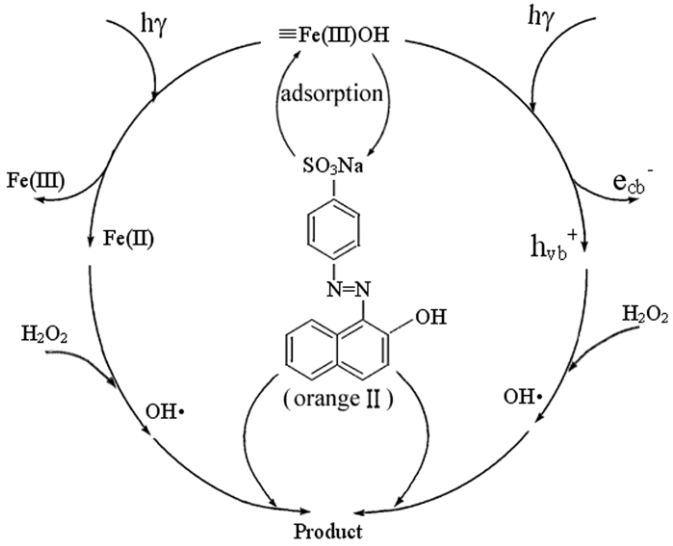

Fig.12 Schematic for the degradation mechanism of orange II using as-prepared γ-FeOOH as photocatalyst

4. Conclusions

Lepidocrocite samples with different degrees of crystallization were obtained by varying the amount of oxalic acid under visible light irradiation. With increasing the concentration of oxalic acid, the crystallization of γ-FeOOH gradually decreased. During the oxidation process of Fe(Ⅱ), the Fe(Ⅱ)-oxalate complex could absorb light in the visible regions and produce oxidizing species, leading to the acceleration of the oxidation rate. The higher oxidation rate was favorable for the formation of low crystalline γ-FeOOH. The as-prepared low-crystalline lepidocrocite samples had large specific surface area, which showed higher adsorption and photocatalytic activity toward the

photodegradation of orange II. Based on the results obtained, it was proposed that lepidocrocites catalyzed the decomposition of H_2O_2 to form hydroxyl radicals (OH•), which contributed most to the oxidation and degradation of orange II

Acknowledgment

This work was supported by the National Natural Science Foundation of China (21477032, 21277040), by the Natural Science Foundation of Hebei Province (B2013205069, B2012205041), by the Key Laboratory of Photochemical Conversion and Optoelectronic Materials, TIPC, CAS (PCOM201110) for financial support.

References

1 J. Lei, C.S. Liu, F.B. Li, X.M. Li, S.G. Zhou, T.X. Liu, M.H. Gu and Q.T. Wu, J. Hazard.Mater., 2006, 137, 1016-1024.

2 W. Li, Y. Wang and A. Irini, Chem. Eng. J., 2014, 244, 1-8.

3 C. Siffert and B. Sulzberger, Langmuir, 1991, 7, 1627-1634.

4 B.C. Faust and J. Allen, Environ. Sci. Technol., 1993, 27, 2517-2522.

5 M.E. Balmer and B. Sulzberger, Environ. Sci. Technol., 1999, 33, 2418-2424.

6 P. Mazellier and B. Sulzberger, Environ. Sci. Technol., 2001, 35, 3314-3320.

7 F. B. Li, X.Z. Li, X.M. Li, T.X. Liu and J. Dong, J.Colloid Interface Sci., 2007, 311, 481- 490.

8 F. Li , X. Wang, Y. Li , C. Liu, F. Zeng, L. Zhang, M. Hao and H. Ruan, J.Colloid Interf. Sci., 2008, 321, 332-341.

9 P. Borer, S.J. Hug, B. Sulzberger, S.M. Kraemer and R. Kretzschmar, J. Phys. Chem. C, 2007,111, 10560-10569.

10 Y. Lin, Y.u Wei and Y. Sun, J. Mol. Catal. A: Chem., 2012, 353– 354, 67- 73.

11 R. Chen, H. Chen, Y. Wei and D. Hou, J. Phys. Chem. C , 2007,111,16453-16459.

12 R. Chen, G. Song and Y. Wei, J. Phys. Chem. C, 2010, 114,13409-13413.

13 H. Liu, Y.Wei and Y. Sun, J. Mol. Catal. A: Chem., 2005, 226,135-140 .

14 S.P. Pablo, A.O. Victor, L.S. Flavio and A.L. Versiane, Biochem. Eng. J., 2010, 51, 194-197.

15 C. Paipa, M. Mateo, I. Godoy, E. Poblete, M.I. Toral and T. Vargas, Miner. Eng., 2005, 18, 1116-1119.

16 X. Wang, C. Liu, X. Li, F. Li and S. Zhou, J. Hazard. Mater., 2008, 153,426-433.

17 C. Sudalar, G. N. Subbanna and T. R. N. Kutty, J. Phys. Chem. Solids, 2003, 64, 2337-2349.

18 M. Pera-Titus, V. Garcia-Molina, M.A. Ba˜nos, J. Gim´enez and S. Esplugas, Appl. Catal. B, 2004, 47, 219-256.

19 M. L. Kremer, Phys. Chem. Chem. Phys., 1999, 1, 3595-3605.

20 Y. Zhou and Y. Deng, Chemosphere, 1997, 35(9), 2051-2058.

21 J. M. Monteagudo, A. Durán, J.M. Corral, A. Carnicer, J.M. Frades and M.A.Alonso, Chem. Eng. J., 2012, 181-182, 281-288.

22 P. Mazellier and B. Sulzberger, Environ. Sci. Technol., 2001, 35, 3314-3320.

23 G.P. Anipsitakis and D.D. Dionysiou, Environ. Sci. Technol., 2004, 38, 3705-3712.

24 F. Ay and F. Kargy, J. Hazard. Mater., 2010, 179, 622-627.

25 T. Misawa, K. Hashimoto and S. Shimodaira, Corros. Sci., 1974, 14, 131-149.

26 Y. Wang, Y. Zhao, Y. Ma, H. Liu and Y. Wei, J. Mole. Catal. A, 2010, 325, 79- 83.

27 W. Du, Y. Xu and Y. Wang, Langmuir, 2008, 24, 175-181.

28 J. Filip, R. Zboril, O. Schneeweiss, J. Zeman, M. Cernik, P. Kvapil and M. Otyepka, Environ. Sci. Technol., 2007, 41,4367–4374.

29 Y. Ma, S. Meng, M.Qin, H. Liu and Y. Wei, J. Phys. Chem. Solids, 2012, 73, 30–34.

30 X.Yang, H. Cui, Y. Li, J. Qin, R. Zhang and H. Tang, ACS Catal. 2013, 3(3),363-369.

31 H.Cui, X.Yang, Q. Gao, H.Liu, Y.Li, H.Tang and X.Yan, Mater.Lett. 2013, 93, 28-31.

32 X.Yang, J.Qin, Y. Jiang, R. Li, Y. Li and H.Tang, RSC Advances, 2014, 4,18627-18636.

33 Y. Mu, H.Q. Yu, J.C. Zheng and S.J. Zhang, J. Photochem. Photobiol. A, 2004, 163, 311–316.

34 J. H. Deng, J.Y. Jiang, Y.Y. Zhang, X.P. Lin, C.M. Du and Y. Xiong, Appl. Catal. B: Environ., 2008, 84, 468–473.

35 X. Fan, H. Hao, X. Shen, F. Chen and J. Zhang, J. Hazard. Mater., 2011, 190, 493-500.

36 J.J. Wu, M. Muruganandham, J.S. Yang and S.S. Lin, Catal. Commun., 2006, 7, 901-906.